Solar Phys (2010) 263: 209–222
DOI 10.1007/s11207-010-9535-2

Assessing the Accuracy of CME Speed and Trajectory Estimates from STEREO Observations Through a Comparison of Independent Methods

C.J. Davis · J. Kennedy · J.A. Davies

Received: 4 December 2009 / Accepted: 19 February 2010 / Published online: 10 March 2010
© Springer Science+Business Media B.V. 2010

Abstract We have estimated the speed and direction of propagation of a number of Coronal Mass Ejections (CMEs) using single-spacecraft data from the STEREO Heliospheric Imager (HI) wide-field cameras. In general, these values are in good agreement with those predicted by Thernisien, Vourlidas, and Howard in *Solar Phys.* **256**, 111 – 130 (2009) using a forward modelling method to fit CMEs imaged by the STEREO COR2 coronagraphs. The directions of the CMEs predicted by both techniques are in good agreement despite the fact that many of the CMEs under study travel in directions that cause them to fade rapidly in the HI images. The velocities estimated from both techniques are in general agreement although there are some interesting differences that may provide evidence for the influence of the ambient solar wind on the speed of CMEs. The majority of CMEs with a velocity estimated to be below 400 km s^{-1} in the COR2 field of view have higher estimated velocities in the HI field of view, while, conversely, those with COR2 velocities estimated to be above 400 km s^{-1} have lower estimated HI velocities. We interpret this as evidence for the deceleration of fast CMEs and the acceleration of slower CMEs by interaction with the ambient solar wind beyond the COR2 field of view. We also show that the uncertainties in our derived parameters are influenced by the range of elongations over which each CME can be tracked. In order to reduce the uncertainty in the predicted arrival time of a CME at 1 Astronomical Unit (AU) to within six hours, the CME needs to be tracked out to at least 30 degrees elongation. This is in good agreement with predictions of the accuracy of our technique based on Monte Carlo simulations.

Within the set of studied CMEs, there are two clear events that were predicted from the HI data to travel over another spacecraft; *in-situ* measurements at these other spacecraft confirm the accuracy of these predictions. The ability of the HI cameras to image Corotating Interaction Region (CIR)-entrained transients as well as CMEs can result in some ambiguity when trying to distinguishing individual signatures.

Keywords Coronal mass ejection · STEREO · Heliospheric images

C.J. Davis (✉) · J. Kennedy · J.A. Davies
STFC Rutherford Appleton Laboratory, Chilton, Oxfordshire OX11 OQX, UK
e-mail: chris.davis@stfc.ac.uk

1. Introduction

The twin spacecraft of the STEREO mission (Kaiser *et al.*, 2008) were launched in October 2006 and placed into ecliptic heliocentric orbits with orbital radii of approximately 1 AU. One spacecraft is orbiting ahead of the Earth (STEREO-A) and the other behind the Earth (STEREO-B). Each spacecraft is moving away from the Earth such that the spacecraft – Sun – Earth angle increases by approximately 22.5 degrees per year. Each STEREO spacecraft carries a suite of *in-situ* instrumentation (IMPACT, Luhmann *et al.*, 2008, and PLASTIC, Galvin *et al.*, 2008), a transient radio-burst detector (SWAVES, Bougeret *et al.*, 2008), and a suite of imaging telescopes (SECCHI, Howard *et al.*, 2008). SECCHI comprises three sunward-pointing telescopes (two coronagraphs, COR1 and COR2, and an Extreme Ultraviolet Imager, EUVI), and a wide-field white-light instrument (Heliospheric Imager, HI). The latter is mounted on the side of each spacecraft and faces the Sun – Earth line, in particular to image Earth-directed solar density transients (such as CMEs) in the solar wind.

Each Heliospheric Imager (Eyles *et al.*, 2009) consists of two wide-field cameras, HI1 and HI2. HI1 has a 20 degree wide field of view centred at approximately 14 degrees elongation while the outer camera, HI2, has a 70 degree field of view centred at 53.4 degrees elongation. The combined field of view of these cameras enables any transient solar wind features propagating along or near the Sun-Earth line to be tracked out to approximately 1 AU.

Since the launch of the STEREO spacecraft, a variety of methods have been developed to exploit STEREO data to estimate the speed and direction of CMEs erupting from the solar surface (see, *e.g.*, Maloney, Gallagher, and McAteer, 2009; de Koning, Pizzo, and Biesecker, 2009; Thernisien, Vourlidas, and Howard, 2009; Rouillard *et al.*, 2009; Liu *et al.*, 2010). These techniques enable the trajectory of a CME to be forecast relative to a given position in the heliosphere, perhaps most importantly that of the Earth. The techniques are, to a large extent, independent of each other and comparison between them is a useful next step in determining the relative merits of each. The most comprehensive analysis of CME trajectories to date is that conducted by Thernisien, Vourlidas, and Howard (2009), subsequently referred to as TVH09. In their paper, TVH09 presented a survey of 26 CMEs observed in STEREO COR2 coronagraph images between November 2007 and August 2008. They used a forward modelling method in which an assumed distribution of electrons around a geometric flux rope was matched to the observations from COR2 on both STEREO spacecraft, in order to determine the direction of propagation, speed and acceleration of the CME front, as well as the flux rope orientation and length. Their results showed a good agreement with independent measurements of CME speed and direction deduced from SOHO coronagraph observations and presented in the Coordinated Data Analysis Workshop (CDAW) catalogue (Yashiro *et al.*, 2004). TVH09 present their results in terms of a radial velocity, and direction relative to the Sun in terms of a Stonyhurst longitude. In the Stonyhurst system, the zero longitude is set at the intersection of the Sun's equator and central meridian as viewed from Earth. If we are to understand the relative strengths and weaknesses of each CME tracking technique, it is beneficial to compare the results obtained for each against a common data set. We propose that the TVH09 survey should be used as a baseline for comparisons, and we present such a comparison between techniques in this paper. While adopting this approach may not be ideal in all cases for each technique (for example, the technique we adopt in the current study is more suited to Earth-directed CMEs as those events with large Stonyhurst longitudes fade rapidly in the outer HI fields of view) it is nonetheless valuable to have a common data set for such comparisons.

2. Tracking CMEs Using HI

The dominant background signal in any HI image is from sunlight scattered from heliospheric dust, forming the F-corona. Unlike the transient structures in the solar wind, however, this is a slowly varying feature. The dynamic range of the cameras is such that, for an exposure time long enough to reduce the uncertainty in the measurement of the F-corona to below the intensity of the solar transients, it is possible to subtract the F-coronal signal. This can be achieved by constructing a background from the values observed in a given pixel over a period of time longer than the time for which solar transients typically occupy the pixel (say a day or more) or alternatively by differencing adjacent images in a sequence. In practice, a combination of techniques is used in order to minimise the background signal from both the F-corona and the background stars. To enhance the appearance of very faint transient features, adjacent images in the sequence are aligned on the background star-field and subtracted to produce difference images. A detailed description of this process is given in Davies *et al.* (2009).

One consequence of viewing an outward-moving solar transient over such a wide range of elongation angles as is done by HI is that a feature moving with a constant speed in a fixed direction will appear to accelerate as it crosses the field of view. The possibility of such a phenomenon was first pointed out by Sheeley *et al.* (1999) and it has subsequently been exploited to characterise transient features in HI data (see, e.g., Sheeley *et al.*, 2008; Rouillard *et al.*, 2008, 2009; Davis *et al.*, 2009; Davies *et al.*, 2009). The measured elongation as a function of time, $\alpha(t)$, of a solar transient moving radially outward with a constant radial speed V_r at a constant observer – Sun – transient propagation angle, β, is governed by that speed and direction according to the formula

$$\alpha(t) = \operatorname{atan}\left[\frac{V_\mathrm{r} t \sin\beta}{r(t) - V_\mathrm{r}\cos\beta}\right], \tag{1}$$

where r is the radial heliocentric distance of the observer (which for the STEREO spacecraft can be assumed to be constant over the time taken for the transient for cross the HI field of view).

One assumption inherent in this technique is that the light scattered from the CME front, and detected by the HI cameras, has come from a single point. In reality, of course, this signal results from a line-of-sight integration through a 3D structure that can be highly longitudinally extended. Howard and Tappin (2009) investigate the uncertainties introduced with this assumption by considering two distinct CME geometries, an expanding sphere and a radially expanding shell. They conclude that if the sum of the angles α and β is 90 degrees the uncertainty in the distance between the observed and true CME front is zero, and remains below 10% while this sum lies between 56 and 124 degrees. The corresponding uncertainty in β would range from 0 – 15 degrees. The vast majority of the data in our study fell well within this range. As a result, we estimate that the uncertainties introduced by our assumption are more likely to be around 5 degrees on average and would bias the apparent CME trajectory towards the observer at large elongations and away from the observer for small elongations.

An established technique used in the tracking of solar transients is through the creation of time-elongation maps (so called j-maps; see *e.g.* Davies *et al.*, 2009, and references therein). In such maps of intensity (or difference intensity) as a function of elongation and time, transient features moving outward from the Sun appear as distinct traces.

For the purposes of this paper, we are interested in tracking CMEs in the ecliptic plane since our code has been developed to track Earth-directed CMEs. Most of the CMEs in the

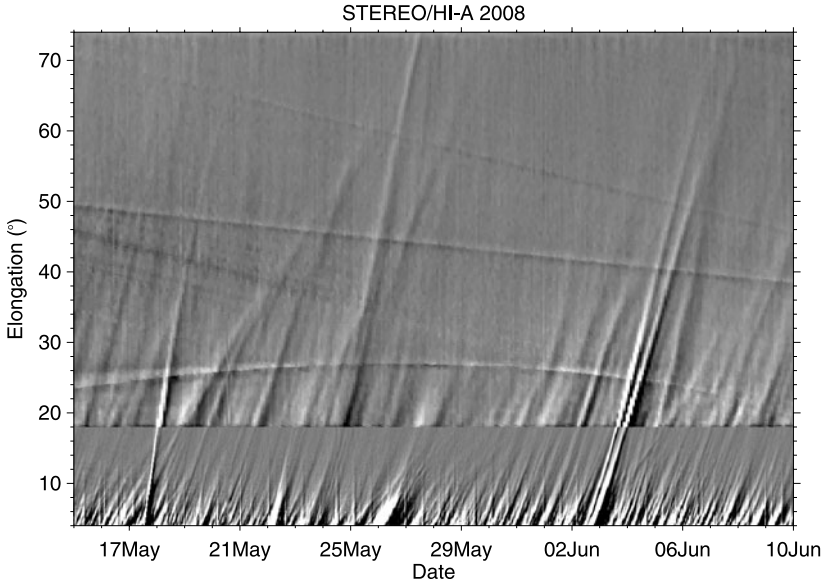

Figure 1 A typical J-map showing the variation of intensity along the ecliptic detected by the HI instrument on STEREO-A as a function of elongation and time. The period covered by this figure – 15th May to the 10th June 2008 – contains the signature of the CME launched on 2nd June 2008 visible as a distinct feature entering the HI field of view on the same day.

TVH09 survey travel along or close to the ecliptic. Six events propagated at higher solar latitudes and are not tracked in our study. The ecliptic corresponds approximately to the central horizontal line across HI images (for the epoch covered by this study). An ecliptic J-map, derived from HI1 and HI2 STEREO-A difference images, is shown in Figure 1 for the interval covering the propagation through the HI field of view of the CME launched on the 2nd June 2008. The CME is manifest in such a plot format as a continuous curve with a positive gradient, the shape of which is determined by its velocity and direction of propagation (as presented in Equation (1)). Note that this is one of the events within the TVH09 survey. For each CME in that survey, a similar J-map is constructed from HI difference images from the appropriate STEREO spacecraft, covering an elongation range extending from the inner sunward edge of the HI1 field of view (around 4 degrees) to the sunward edge of the occulting plate on the far edge of the HI2 field of view (around 74 degrees). The 2nd June 2008 CME can be tracked continuously in the ecliptic plane by HI on STEREO-A from 4.5 to 56.9 degrees.

In this study, the time variation of elongation for each individual transient (*i.e.* its elongation profile) was extracted from the J-map using a manual selection procedure. The speed and direction of each event was then estimated by using Equation (1) to determine the combination of V_{r} and β that produced the best fit to its observed elongation profile. For each CME, uncertainties in the fitted parameters are determined from the values of V_{r} and β that cause the residual in the fit to increase by one standard deviation above the minimum standard deviation (which defines the best fit). It is important to reiterate that this technique enables the radial speed and direction of a CME to be estimated from the observations made from a single spacecraft.

J-maps are constructed using image differencing, as noted previously, in order to enhance the faintest propagating transient features. Therefore, intensity enhancements appear

as light grey/white regions while depletions appear as dark grey/black regions. In the J-maps, propagating transients therefore appear as adjacent light/dark features. The clearest features correspond to the steepest density gradients, usually found at the transition between the plasma associated with the CME leading front and the following plasma cavity. Tracking this part of a CME introduces a small systematic offset in the predicted arrival time of an event. The advantage in creating J-maps from differenced images rather than background subtracted images is that it is possible to track transient features much further across the field of view. The ability to track such events over an extended range of elongations is important in reducing the uncertainties in their characteristics determined from the fitting procedure; we demonstrate this later.

While this technique of deriving the speed and direction of solar wind transients from their elongation variation has been used to characterise individual features in HI data (Rouillard *et al.*, 2008, 2009; Sheeley *et al.*, 2008; Davies *et al.*, 2009; Davis *et al.*, 2009), a statistical survey of such estimates for a larger number of events has not previously been undertaken. In this paper, we present a comparison of our estimates of CME speeds and directions with those derived by TVH09 for a significant number of events.

3. Results

For each of the 26 CMEs presented by TVH09 that were visible in the HI data, we calculated its speed and direction in the ecliptic plane from the HI images using the technique described above. Very few of the events were observed by the HI instruments on both spacecraft; unlike the sunward-pointing instruments, the two HI instruments look towards the Sun – Earth line so a CME will only be visible to both HI instruments if its propagation path is between the two spacecraft. This is not a problem for the technique used since the speed and direction can be estimated from the apparent acceleration of a CME observed from the HI instrument on a single spacecraft. The time-elongation profile for each CME is extracted from the corresponding J-map manually, so each event was traced and fitted at least five times in order to characterise the uncertainty introduced by manual tracing as well as the uncertainty in the fitting itself. Table 1 contains a summary of our estimates of β and V_{r} for each CME. Two estimates of the uncertainty are quoted for each value of V_{r} and β. The first is the standard deviation of the parameters retrieved from the 5 or more fits (illustrating the variability introduced by repeated manual tracing of the same event). We have, using the method defined above, associated errors in β and V_{r} for each fit, from which we compute a second uncertainty being the mean of those (in brackets). The largest of the two uncertainty values quoted for each event is used in all plots.

Figure 2a shows a comparison of CME propagation angles (presented in Stonyhurst longitude) derived from the forward modelling method (FMM) of TVH09 compared with those obtained from the HI observations using the technique outlined above. Most of the events in the TVH09 survey cover a range of latitudes which includes the ecliptic plane and so a comparison with the HI velocities (calculated along the ecliptic plane) can be made, although this may introduce a small discrepancy in the values measured by the two techniques if a latitudinal gradient in velocity exists. There are a few events that propagate along far higher solar latitudes and so a direct comparison of the characteristics of these events cannot be made. In general, there is good agreement between the CME propagation angles estimated from both techniques although the absence of quoted uncertainties for each event in the TVH09 results makes it difficult to calculate the significance of the correlation. TVH09 quote an average uncertainty of 4 degrees and a maximum uncertainty of 17 degrees in longitude. The largest

Table 1 A comparison of derived speeds and directions for 20 CMEs estimated from two independent techniques. Date refers to the date used to identify the events in the TVH09 survey. HI values denote the estimates derived from HI images described in this paper, while FMM values denote those derived by TVH09 from the STEREO COR2 data. The HI cameras are optimised to image CMEs that are propagating in the vicinity of the Sun – Earth line and so were unable to image six of the CMEs in the TVH09 survey that were either propagating at a high latitude or for which their large predicted angles resulted in the CME being too far from the spacecraft to be imaged by the time it would have appeared in the HI field of view.

Date	S/C	HI speed ($km\,s^{-1}$)	HI direction (degrees)	FMM speed ($km\,s^{-1}$)	FMM direction (degrees)
04 Nov 2007	A	428 ± 10 (12)	-42 ± 6 (4)	216	−44
16 Nov 2007	B	364 ± 61 (78)	98 ± 11 (13)	345	123
04 Dec 2007	B	339 ± 8 (15)	55 ± 2 (5)	265	71
16 Dec 2007	A	174 ± 20 (14)	-81 ± 9 (6)	325	−144
31 Dec 2007	A	869 ± 260 (80)	-94 ± 31 (11)	972	−80
02 Jan 2008	A	388 ± 14 (9)	-55 ± 5 (3)	731	−51
23 Jan 2008	–	Not tracked	Not tracked	442	−160
29 Jan 2008	B	Not tracked	Not tracked	246	107
04 Feb 2008	A	432 ± 12 (7)	-37 ± 6 (4)	598	−21
12 Feb 2008	B	Not tracked	Not tracked	249	93
13 Feb 2008	A	238 ± 5 (4)	-44 ± 5 (4)	225	−18
15 Feb 2008	A	236 ± 3 (3)	-46 ± 4 (3)	230	−73
24 Feb 2008	A	360 ± 111(132)	-67 ± 36 (24)	244	−122
17 Mar 2008	B	283 ± 4 (9)	36 ± 4 (8)	221	40
18 Mar 2008	A	Not tracked	Not tracked	340	−83
25 Mar 2008	A	1021 ± 96 (57)	-93 ± 3 (3)	1127	−83
05 Apr 2008	B	1060 ± 146 (161)	111 ± 3 (10)	1043	126
26 Apr 2008	A	649 ± 70 (60)	-49 ± 17 (12)	741	−21
17 May 2008	A	776 ± 37 (23)	-52 ± 3 (2)	986	−45
24 May 2008	B	381 ± 3 (3)	2 ± 1 (2)	331	39
02 Jun 2008	A	364 ± 6 (2)	-24 ± 2 (1)	265	−37
12 Jun 2008	A	508 ± 62 (101)	-92 ± 5 (7)	319	−102
26 Jun 2008	–	Not tracked	Not tracked	389	−147
07 Jul 2008	A	549 ± 19 (10)	-31 ± 4 (2)	292	−23
31 Jul 2008	–	Not tracked	Not tracked	288	141
07 Aug 2008	A	337 ± 19 (18)	-44 ± 6 (5)	215	−54

uncertainties from our fits generally occur for larger angles since these events tend to be propagating further from the Sun – spacecraft line, resulting in their rapid fading in the HI images. Also, these events are more prone to larger systematic errors as discussed earlier, since they are propagating at large angles from the observer. In total, six of the events in the THV09 survey were not observed by HI either because they were not propagating along the ecliptic plane or they were travelling at a large angle to the Sun – spacecraft line.

Figure 2b shows a similar comparison of the radial speeds calculated from both techniques. Again, the largest uncertainties occur for events that propagate in directions that take them away from the Sun – spacecraft line. While there is good agreement between the radial speeds calculated from the two techniques, in general, the overall correlation is somewhat worse than for the propagation angles presented in Figure 2a. The majority of

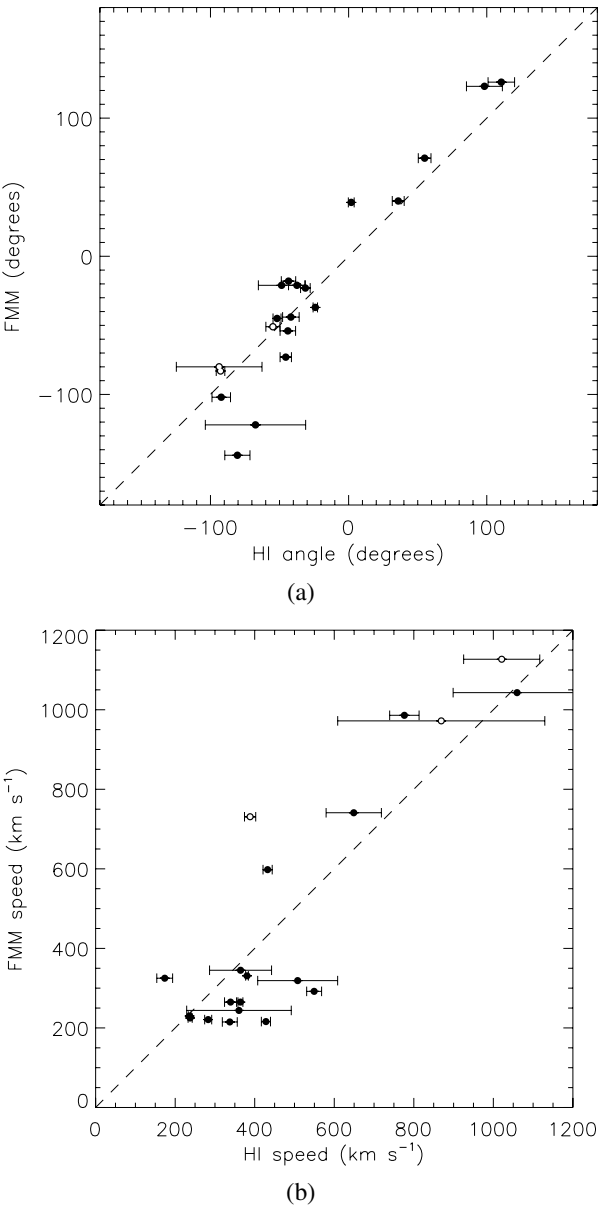

Figure 2 (a) Propagation angles derived from CMEs using the forward modelling method (FMM) of TVH09 compared with the results from the HI elongation variation fitting method. There is good agreement for the 20 events observed by both COR2 and HI, with the largest uncertainties in the HI method occurring at larger angles. The shading of the points indicates those events that were estimated to be accelerating (black) and decelerating (white) in the TVH09 survey. (b) The same as Figure 2a but this time showing a comparison of derived velocities. The agreement is not as good as for the derived angles with the FMM velocity being lower than the HI velocity for most CMEs below 400 km s^{-1} (in the COR2 field of view) and most FMM velocities being slightly higher than HI velocities for CMEs above 400 km s^{-1} in COR2. The shading of the points indicates those events that were estimated to be accelerating (black) and decelerating (white) in the TVH09 survey.

CMEs with a velocity estimated to be below 400 km s^{-1} in the COR2 field of view have higher estimated velocities in the HI field of view, while, conversely, those with COR2 velocities estimated to be above 400 km s^{-1} have lower estimated HI velocities. This is consistent with slower CMEs being accelerated by their interaction with the ambient solar wind while faster CMEs are decelerated. Similar conclusions have been reached by previous authors (see, *e.g.*, Gopalswamy *et al.*, 2000; Yashiro *et al.*, 2004; Jones *et al.*, 2007; Wen *et al.*, 2008).

TVH09 derive both a speed and an acceleration for each of the CMEs. The points in Figures 2a and 2b indicate those events showing acceleration (solid black dots) and deceleration (white dots) according to the TVH09. All three of the events that are seen to be decelerating in the COR2 field of view (white dots) travel at lower speeds in the HI field of view while the majority of those events seen to be accelerating in COR2 are travelling faster by the time they are observed in HI.

The technique used for HI assumes that each event has a constant radial speed and direction when in the HI field of view. Although comparison with *in-situ* measurements (see, *e.g.*, Davis *et al.*, 2009; Rouillard *et al.*, 2009) has shown that the assumptions inherent in the HI technique are reasonable in a few specific examples, it is still a possibility that a CME will undergo genuine acceleration while in the HI field of view and this would also introduce a systematic error in the fitted values. Since the estimates for the direction of propagation are consistent between the two techniques, a combined process may prove useful. Tracking a CME in the COR2 images would yield a direction of propagation which could be used to further constrain the fit in the HI CME observations and allow a velocity profile across the HI field of view to be estimated. A similar technique has been demonstrated by Morrill *et al.* (2009). We intend to investigate such a combined technique, but it is beyond the scope of the current paper.

The uncertainties quoted in the HI results correlate well with the elongation range over which an event can be tracked by the HI cameras. For events that can only be tracked out to smaller elongations, the two-parameter fit to the elongation variation (based on Equation (1)) is less well constrained resulting in a greater uncertainty in the best-fit values. If this technique is to be used for accurate forecasting, it is important to characterise the extent to which an event must be tracked before the fitting process is well constrained.

The relationship between the elongation extent over which a CME is tracked and the estimated uncertainty in the fitted parameters is presented in Figures 3a and 3b for the angle and speed, respectively. The former is plotted in terms of the maximum observable elongation; all events were tracked from the inner edge of the HI1 field of view (*i.e.* a minimum elongation of about 4 degrees). For the propagation angle there is a distinct improvement (to below ten degrees) in fitting accuracy once a CME can be tracked out to elongations exceeding 30 degrees in the HI field of view. For a CME propagating along the ecliptic, this corresponds to a track that extends beyond 12 degrees into the HI2 field of view. The relationship between the maximum elongation of observation and the uncertainty in radial speed (Figure 3b) is somewhat less clear, but in terms of obtaining the accuracy required for a space-weather forecast it is the uncertainty in arrival time that is of importance. Figure 4 shows the relationship between maximum elongation and uncertainty in arrival time at 1 AU. While depending on the direction of propagation, it can be seen that, in general, tracking a CME out to an elongation of more than 30 degrees will constrain the uncertainty in arrival time at 1 AU to within six hours. These results are consistent with those of Williams *et al.* (2009), who performed a Monte Carlo analysis of simulated elongation variations to investigate the efficacy of this technique. The authors found that, although the accuracy of the results does depend to a large extent on the values of the velocity and propagation direction that define the simulated transient, it is necessary to fit its track to elongations beyond the maximum extent of the HI1 field of view to gain a viable estimate of these parameters.

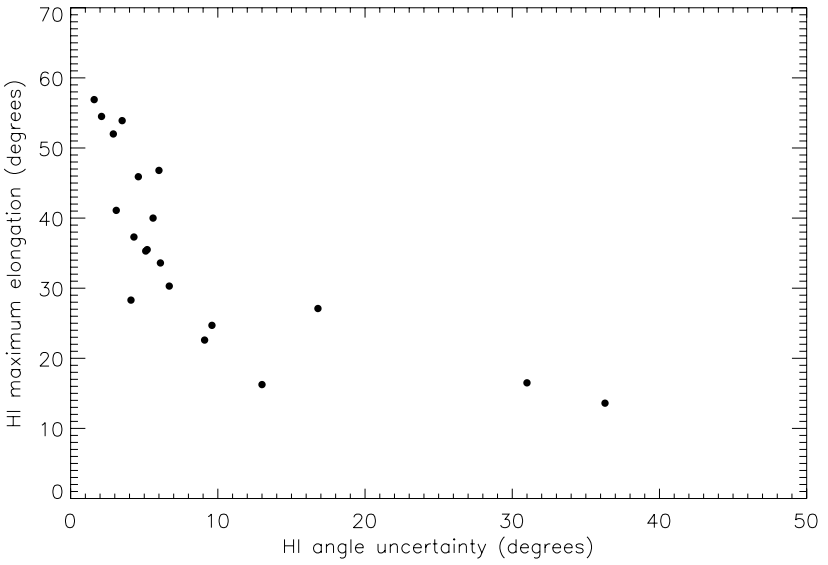

(a)

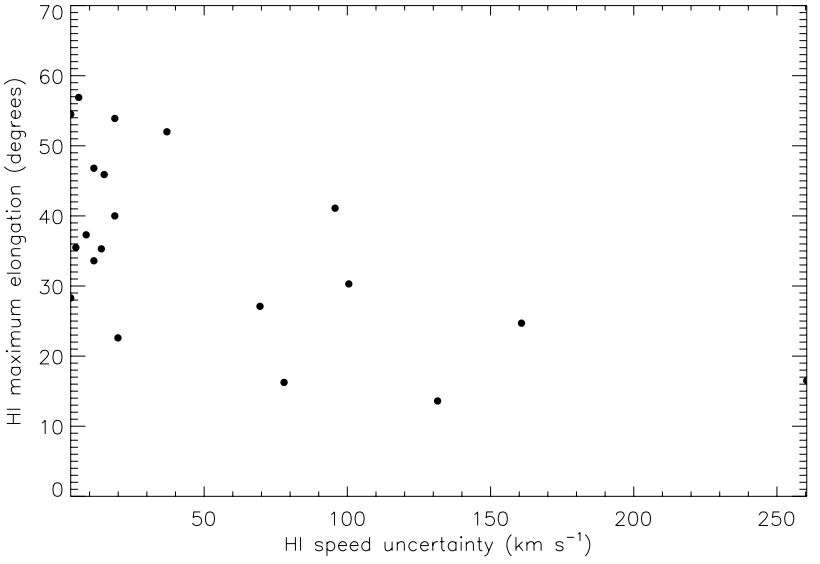

(b)

Figure 3 (a) The maximum elongation to which each event could be observed plotted against the resulting uncertainty in the best-fit values of propagation angle. The fitting is more tightly constrained for those events that can be tracked to larger elongations in the HI cameras. The results of this survey indicate that an event needs to be tracked to an elongation of at least 30 degrees before the uncertainty in the direction of propagation is reduced to within 7 degrees. (b) The same as for Figure 3a but this time showing maximum elongation *versus* uncertainty in the estimated speed of each CME. Again the uncertainty decreases as the elongation over which an event is tracked increases. The large spread in CME speeds within this survey result in a larger scatter than for the angles shown in Figure 3a.

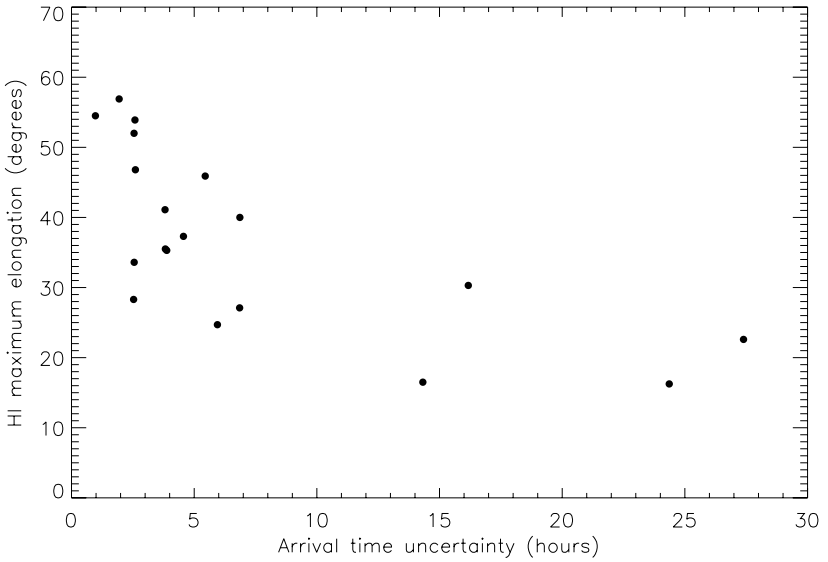

Figure 4 Maximum elongation *versus* estimated uncertainty in arrival time at 1 AU derived from the uncertainty values shown in Figure 3b. A CME needs to be tracked to elongations in excess of approximately 30 degrees in order for the uncertainty in arrival time to be within six hours.

4. *In-Situ* Measurements

As discussed by TVH09, a subset of these CMEs travelled in directions such that they impacted one or other of the STEREO spacecraft which provide *in-situ* measurements of the solar wind. Such ground-truth provides an independent test with which to compare the predicted arrival times.

Of the four CMEs from this study that have been identified in the STEREO IMPACT *in-situ* data, two cannot be unambiguously matched up with the fronts observed by HI because the particle and magnetic field data exhibit excessive structure due to the proximity of the heliospheric current sheet (HCS) and associated CIRs. The distinguishing of CME and CIR-associated signatures in the visible-light images and *in-situ* observations is beyond the scope of this paper but is being tackled separately by other authors. A complex sequence of CME/CIR interactions during the early part of February 2008 is currently under study (Rouillard, private communication) while Wood and Howard (2009) investigate the event of 26th April 2008. The latter study confirms the results of TVH09 that this event impacted STEREO-B. The results of the application of our technique alone are less conclusive for this event since, in the outer HI2 field of view, the CME signature becomes confused with the signature of a CIR-associated transient.

Inspection of the angles retrieved from our fitting technique, reveals two clear candidate CMEs from the set under study that passed within 10 degrees of spacecraft capable of making *in-situ* observations. The first was the event of 24th May 2008, which was predicted (using HI on the STEREO-B spacecraft) to travel at an angle of 1 ± 2 degrees from the Sun – Earth line. This is highly suggestive of its passage over the *Advanced Composition Explorer* (ACE, Stone *et al.*, 1998) satellite, which is positioned ahead of the Earth at the first Lagrangian point, L1. The second event, that of the 2nd June 2008, was observed by

HI on the STEREO-A spacecraft to propagate in a direction that would take it within 1 ± 2 degrees of the STEREO-B spacecraft (this CME we consider first).

Figure 1 shows the J-map including the CME of the 2nd June 2008. The speeds and directions estimated for all of the events in this study were calculated by tracking the most prominent signature of each in the J-maps – this being the trailing edge of the CME front, where the steep density gradient shows up as a sharp transition between positive (light) and negative (dark) contour levels. For comparison with *in-situ* measurements for the two events listed above, the HI signature of each was examined in more detail with its speed and direction derived from the elongation variation of three features: the leading edge of the CME front, the trailing edge of the CME front (as inferred from the light/dark transition), and the leading edge of the core material.

The CME of the 2nd June 2008 was deduced from HI data taken by the STEREO-A spacecraft to be propagating in a direction that would take it over STEREO-B. The IMPACT instrument suite on STEREO-B first detected its arrival at 15:36 UT on the 6th June (in terms of the density enhancement corresponding to its initial front), with the magnetic flux rope signature being first detected at 22:15 UT on the same day. The event had passed over the spacecraft by 12:32 UT on the 7th June.

The three features corresponding to the leading and trailing edges of the CME front together with the leading edge of the CME core material were predicted, using our technique based on the HI observations, to arrive at STEREO-B at $00{:}38 \pm 2{:}00$, $03{:}15 \pm 2{:}00$, $16{:}00 \pm 2{:}00$ UT on the 7th June 2008 respectively. Figure 5 shows particle and magnetic field data from IMPACT on STEREO-B with these arrival times overlaid as vertical dotted lines (with uncertainties shown as shaded areas, note these overlap). The *in-situ* data reveal an initial rise in the plasma number density, followed by a magnetic field enhancement and rotation accompanied by a decrease in solar wind speed and number density, and a trailing density enhancement. Such *in-situ* signatures are characteristic of a typical three part CME with embedded flux rope.

For the event of the 24th May 2008 and imaged by HI-B, three CME features, similar to those in the event described previously, were predicted to pass over the ACE spacecraft at $04{:}37 \pm 1{:}00$, $08{:}46 \pm 1.00$ and $13{:}04 \pm 1{:}00$ UT on the 28th May respectively. Figure 6 shows the magnetic field and solar wind data from the ACE spacecraft for this interval. The predicted arrival times of the three CME features are each shown as a dashed line within a shaded area representing the uncertainty in their predicted arrival at the spacecraft. There is good agreement between the predicted arrival times and the detection by ACE of an initial enhancement in plasma number density, a flux rope, and the density increase corresponding to the CME core material.

5. Conclusions

We have estimated the speed and direction of a number of CMEs from their elongation variation seen in data from the STEREO HI instruments. In general, these values were in good agreement with those predicted by Thernisien, Vourlidas, and Howard (2009) using a forward modelling method to estimate the propagation characteristics of CMEs seen in the STEREO coronagraphs. As the events in this data set were chosen because of their clarity in COR2 images, it is encouraging that the directions of the CMEs predicted by both techniques are in very good agreement despite many of the CMEs in this study travelling in directions that caused them to fade rapidly in the HI images. Discrepancies in velocity between the two methods provide evidence for the acceleration of slow CMEs and deceleration of fast CMEs by interaction with the ambient solar wind.

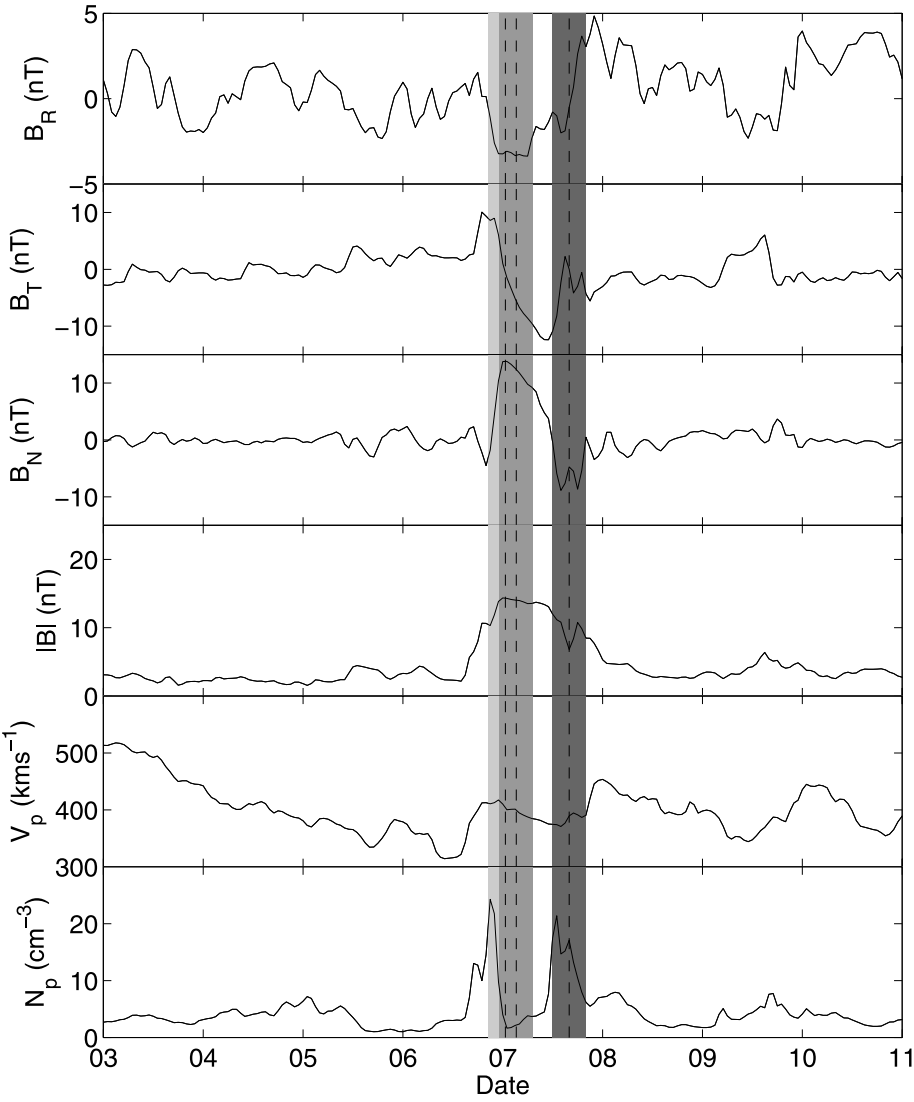

Figure 5 Data from the *in-situ* instrumentation onboard the STEREO-B spacecraft from the 3rd to 11th June 2008. The top four panels show the radial, tangential and normal components together with the magnitude of the interplanetary magnetic field (B_{R}, B_{N}, B_{T} and $|B|$, respectively). The lower two panels show the solar wind velocity (V_{p}) and the solar wind proton density (N_{p}). The predicted arrival at the spacecraft of three CME features seen by the HI cameras are over plotted as dashed lines surrounded by a shaded area indicating the estimated uncertainty in arrival time.

We have shown that the uncertainties in our fitting technique are influenced by the maximum elongations to which the CMEs can be tracked. In order to reduce the uncertainty in the predicted arrival time of a CME at 1 AU to within six hours, a CME needs to be tracked to at least 30 degrees elongation.

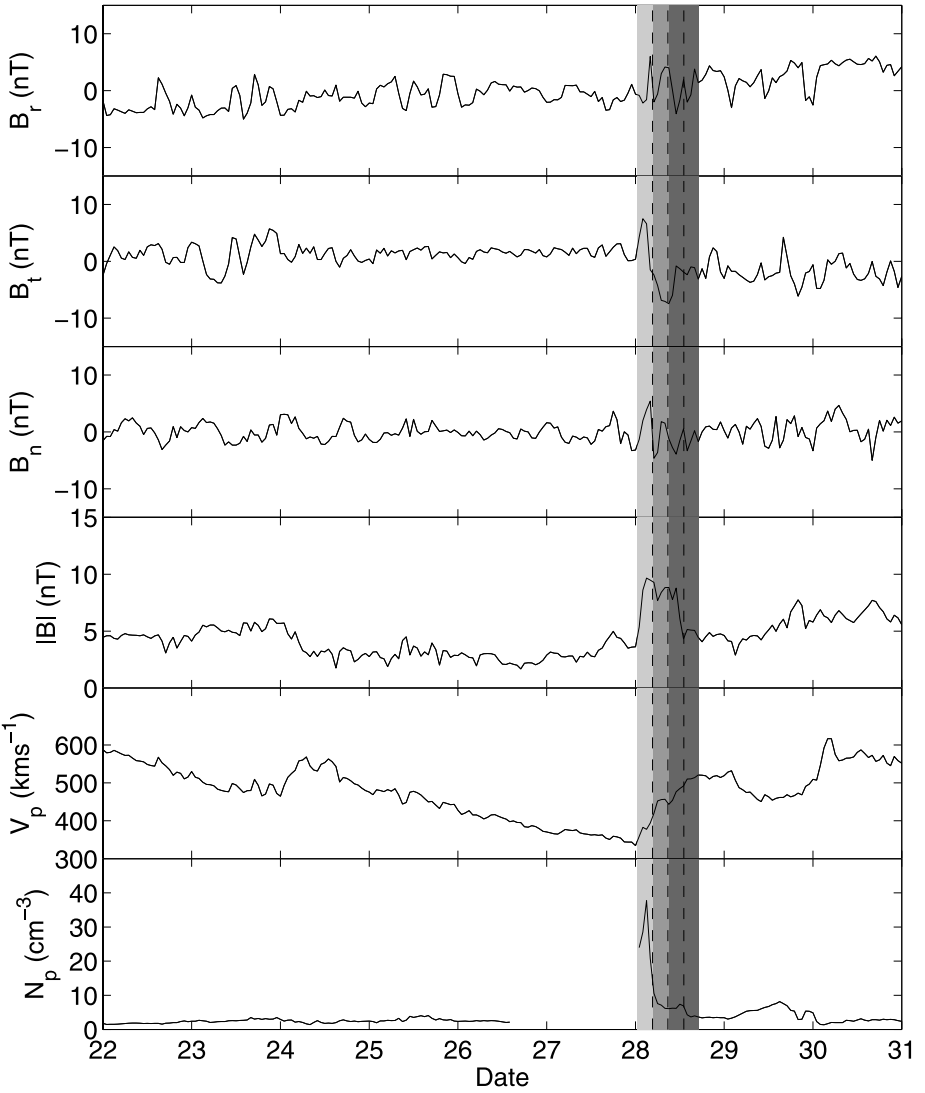

Figure 6 Data from the *in-situ* instrumentation onboard the ACE spacecraft from the 22nd to the 31st May 2008. The top four panels show the radial, tangential and normal components together with the magnitude of the interplanetary magnetic field (B_{R}, B_{N}, B_{T} and $|B|$, respectively). The lower two panels show the solar wind velocity (V_{p}) and the solar wind proton density (N_{p}). The predicted arrival at the spacecraft of three CME features seen in the HI cameras are over plotted as dashed lines surrounded by a shaded area indicating the estimated uncertainty in arrival time.

Within our study there are two clear events in the HI data that were predicted to travel over another spacecraft, and *in-situ* measurements confirmed the accuracy of these predictions.

Acknowledgements The authors wish to thank the STEREO IMPACT/MAG team, the ACE/MAG instrument team and science center and the CDAW data center. The Heliospheric Imager instrument was developed by a collaboration which included the Rutherford Appleton Laboratory and the University of Birmingham,

both in the UK, and the Centre Spatial de Liège (CSL), Belgium and the US Naval Research Laboratory (NRL), Washington DC, USA. The STEREO/SECCHI project is an international consortium of the Naval Research Laboratory (USA), Lockheed Martin Solar and Astrophysics Lab (USA), NASA Goddard Space Flight Center (USA), Rutherford Appleton Laboratory (UK), University of Birmingham (UK), Max-Planck-Institut für Sonnensystemforschung (Germany), Centre Spatial de Liège (Belgium), Insititut d'Optique Théorique et Appliquée (France) and Institut d'Astrophysique Spatiale (France).

References

Bougeret, J.L., Goetz, K., Kaiser, M.L., Bale, S.D., Kellogg, P.J., Maksimovic, M., Monge, N., Monson, S.J., Astier, P.L., Davy, S., *et al.*: 2008, *Space Sci. Rev.* **136**, 487 – 528.

Davies, J.A., Harrison, R.A., Rouillard, A.P., Sheeley, N.R., Perry, C.H., Bewsher, D., Davis, C.J., Eyles, C.J., Crothers, S.R., Brown, D.S.: 2009, *Geophys. Res. Lett.* **36**, L02102.

Davis, C.J., Davies, J.A., Lockwood, M., Rouillard, A.P., Eyles, C.J., Harrison, R.A.: 2009, *Geophys. Res. Lett.* **36**, L08102.

de Koning, C.A., Pizzo, V.J., Biesecker, D.A.: 2009, *Solar Phys.* **256**, 167 – 181.

Eyles, C.J., Harrison, R.A., Davis, C.J., Waltham, N.R., Shaughnessy, B.M., Mapson-Menard, H.C.A., Bewsher, D., Crothers, S.R., Davies, J.A., Simnett, G.M., *et al.*: 2009, *Solar Phys.* **254**, 387 – 445.

Galvin, A.B., Kistler, L.M., Popecki, M.A., Farrugia, C.J., Simunac, K.D.C., Ellis, L., Mobius, E., Lee, M.A., Boehm, M., Carroll, J., *et al.*: 2008, *Space Sci. Rev.* **136**, 437 – 486.

Gopalswamy, N., Lara, A., Lepping, R.P., Kaiser, M.L., Berdichevsky, D., St. Cyr, O.C.: 2000, *Geophys. Res. Lett.* **27**, 145 – 148.

Howard, R.A., Moses, J.D., Vourlidas, A., Newmark, J.S., Socker, D.G., Plunkett, S.P., Korendyke, C.M., Cook, J.W., Hurley, A., Davila, J.M., *et al.*: 2008, *Space Sci. Rev.* **136**, 67 – 115.

Howard, T.A., Tappin, S.J.: 2009, *Space Sci. Rev.* **147**, 31 – 54.

Jones, R.A., Breen, A.R., Fallows, R.A., Canals, A., Bisi, M.M., Lawrence, G.: 2007, *J. Geophys. Res.* **112**, A08107.

Kaiser, M.L., Kucera, T.A., Davila, J.M., St. Cyr, O.C., Guhathakurta, M., Christian, E.: 2008, *Space Sci. Rev.* **136**, 5 – 16.

Liu, Y., Davies, J.A., Luhmann, J.G., Vourlidas, A., Bale, S.D., Lin, R.P.: 2010, *Astrophys. J. Lett.* **710**, 82 – 87.

Luhmann, J.G., Curtis, D.W., Schroeder, P., McCauley, J., Lin, R.P., Larson, D.E., Bale, S.D., Sauvaud, J.A., Aoustin, C., Mewaldt, R.A., *et al.*: 2008, *Space Sci. Rev.* **136**, 117 – 184.

Maloney, S.A., Gallagher, P.T., McAteer, R.T.J.: 2009, *Solar Phys.* **256**, 149 – 166.

Morrill, J.S., Howard, R.A., Vourlidas, A., Webb, D.F., Kunkel, V.: 2009, *Solar Phys.* **259**, 179 – 197.

Rouillard, A.P., Davies, J.A., Forsyth, R.J., Rees, A., Davis, C.J., Harrison, R.A., Lockwood, M., Bewsher, D., Crothers, S.R., Eyles, C.J., Hapgood, M., Perry, C.H.: 2008, *Geophys. Res. Lett.* **35**, L10110.

Rouillard, A.P., Davies, J.A., Forsyth, R.J., Savani, N., Sheeley, N.R., Thernisien, A., Zhang, T.-L., Howard, R.A., Anderson, B., Carr, C.M., *et al.*: 2009, *J. Geophys. Res.* **114**, A07106.

Sheeley, N.R., Walters, J.H., Wang, Y.-M., Howard, R.A.: 1999, *J. Geophys. Res.* **104**, 24739 – 24767.

Sheeley, N.R., Herbst, A.D., Palatchi, C.A., Wang, Y.-M., Howard, R.A., Moses, J.D., Vourlidas, A., Newmark, J.S., Socker, D.G., Plunkett, S.P., *et al.*: 2008, *Astrophys. J.* **675**, 853 – 862.

Stone, E.C., Frandsen, A.M., Mewaldt, R.A., Christian, E.R., Margolies, D., Ormes, J.F., Snow, F.: 1998, *Space Sci. Rev.* **86**, 1 – 22.

Thernisien, A., Vourlidas, A., Howard, R.A.: 2009, *Solar Phys.* **256**, 111 – 130.

Williams, A.O., Davies, J.A., Milan, S.E., Rouillard, A.P., Davis, C.J., Perry, C.H., Harrison, R.A.: 2009, *Ann. Geophys.* **27**, 4359 – 4368.

Yashiro, S., Gopalswamy, N., Michalek, G., St. Cyr, O.C., Plunkett, S.P., Rich, N.B., Howard, R.A.: 2004, *J. Geophys. Res.* **109**, A07105.

Wen, Y.Y., Wang, J.X., Zhao, H., Maia, D.J.F.: 2008, *Adv. Space Res.* **42**, 852 – 857.

Wood, B.E., Howard, R.A.: 2009, *Astrophys. J.* **702**, 901 – 910.